



**HAL**  
open science

## Experimental evidence for long-distance electrodynamic intermolecular forces

Mathias Lechelon, Yoann Meriguet, Matteo Gori, Sandra Ruffenach, Iliaria Nardecchia, Elena Floriani, Dominique Coquillat, Frederic Teppe, Sébastien Mailfert, Didier Marguet, et al.

► **To cite this version:**

Mathias Lechelon, Yoann Meriguet, Matteo Gori, Sandra Ruffenach, Iliaria Nardecchia, et al.. Experimental evidence for long-distance electrodynamic intermolecular forces. 2021. hal-03259009v2

**HAL Id: hal-03259009**

**<https://hal.science/hal-03259009v2>**

Preprint submitted on 12 Oct 2021 (v2), last revised 17 Feb 2022 (v5)

**HAL** is a multi-disciplinary open access archive for the deposit and dissemination of scientific research documents, whether they are published or not. The documents may come from teaching and research institutions in France or abroad, or from public or private research centers.

L'archive ouverte pluridisciplinaire **HAL**, est destinée au dépôt et à la diffusion de documents scientifiques de niveau recherche, publiés ou non, émanant des établissements d'enseignement et de recherche français ou étrangers, des laboratoires publics ou privés.

1  
2  
3

# Experimental evidence for long-distance electrodynamic intermolecular forces

Mathias Lechelon,<sup>1,2</sup> Yoann Meriguet,<sup>3,4</sup> Matteo Gori,<sup>1,5</sup> Sandra Ruffenach,<sup>4</sup>  
Ilaria Nardecchia,<sup>1,2</sup> Elena Floriani,<sup>1</sup> Dominique Coquillat,<sup>4</sup>  
Frédéric Teppe,<sup>4</sup> Sébastien Mailfert,<sup>2</sup>  
Didier Marguet,<sup>2</sup> Pierre Ferrier,<sup>2</sup> Luca Varani,<sup>3</sup>  
James Sturgis,<sup>6</sup> Jeremie Torres,<sup>3,\*</sup> Marco Pettini,<sup>1,\*</sup>

<sup>1</sup> Aix-Marseille Univ, Université de Toulon, CNRS, Marseille, France  
Centre de Physique Théorique, CNRS, Marseille, France

<sup>2</sup> Centre d'Immunologie de Marseille-Luminy, Aix-Marseille Université,  
CNRS, Inserm, Marseille, France

<sup>3</sup> Institut d'Electronique et des Systèmes, University of Montpellier - CNRS, Montpellier, France

<sup>4</sup> Laboratoire Charles Coulomb, University of Montpellier - CNRS, Montpellier, France

<sup>5</sup> Quantum Biology Lab, Howard University, 2400 6th St NW, Washington, DC 20059, USA

<sup>6</sup> Laboratoire d'Ingenierie des Systèmes Macromoléculaires, Aix-Marseille Univ,  
CNRS, Marseille, France

\* Corresponding authors: jeremie.torres@umontpellier.fr; marco.pettini@cpt.univ-mrs.fr

4 **Both Classical and Quantum Electrodynamics predict the existence of dipole-**  
5 **dipole long-range electrodynamic intermolecular forces, however these have**  
6 **never been hitherto experimentally observed. The discovery of completely**  
7 **new and unanticipated forces acting between biomolecules could have con-**  
8 **siderable impact on our understanding of the dynamics and functioning of the**  
9 **molecular machines at work in living organisms. Here, using two independent**  
10 **approaches, we demonstrate experimentally for the first time the activation of**

11 **resonant electrodynamic intermolecular forces. By resorting to fluorescence**  
12 **correlation spectroscopy - to study molecular diffusion in solution - a clus-**  
13 **tering phase transition induced by these electrodynamic forces is detected. By**  
14 **resorting to Terahertz spectroscopy, it is found that the oscillation frequency of**  
15 **the molecular dipoles changes with the intermolecular distance as expected in**  
16 **presence of these electrodynamic forces. This is an unprecedented experimen-**  
17 **tal *proof of principle* of a physical phenomenon that, having been observed for**  
18 **bio-macromolecules and with a long-range of action (up to  $1000 \text{ \AA}$ ), could be**  
19 **of importance for biology. Therefore, in addition to thermal fluctuations that**  
20 **drive molecular motion randomly, these resonant (and thus selective) electro-**  
21 **dynamic forces may contribute to molecular encounters in the crowded cellu-**  
22 **lar space. We anticipate our findings will provide a basis for future systematic**  
23 **deepening of physical aspects of the reported phenomena and for future sys-**  
24 **tematic assessment of the relevance of electrodynamic forces in shaping the**  
25 **dynamics of biomolecular encounters and recognition in biology.**

## 26 **Introduction**

27 Beyond the strong interest for fundamental physics of observing intermolecular dipole-dipole  
28 electrodynamic (ED) forces, this experimental study to detect these forces was highly motivated  
29 by their possible role at the molecular level in biology. Indeed, from a physicists point of view,  
30 living matter offers a wealth of fascinating dynamic phenomena involving biomolecules (pro-  
31 teins and nucleic acids) organized in an intricate and complex network of biochemical interac-  
32 tions providing astonishing efficiency. In numbers, a human cell at any given time may contain  
33 about 130,000 binary interactions between proteins [1], of which about 34,000 unique human  
34 protein-protein interactions are already listed on databases [2]. The forces hitherto considered

35 in biological contexts are of (quasi-) electrostatic nature (chemical-, and hydrogen-bonds, bare  
36 Coulomb, Van-der-Waals London, Hamaker-forces) and are limited to a range of action shorter  
37 than  $10 \text{ \AA}$  due to Debye screening by small freely moving ions in the intracellular water. Such  
38 interactions are relevant for stereo-specific, "lock-and-key" and "induced-fit" interactions at  
39 short distances but hardly effective to recruit distant molecules. Thus, understanding how the  
40 right molecule gets to the right place, at the right moment, in the right cascade of events of  
41 any biological action is one of the most striking challenges. Fundamentally, it is assumed that  
42 this network of interactions is dominated by random molecular diffusion throughout the cellular  
43 spaces in which, sooner or later, a molecule will encounter its cognate partners. However, free  
44 diffusion is considerably slowed down in a highly crowded environment [3] as in the case of  
45 the cell interior. Moreover, when diffusion measurements are performed in complex molecular  
46 organizations such as those of living cells, most of the biomolecules show anomalous rather  
47 than Brownian diffusion [4, 5]. Furthermore, structuring of the cytosol into phase-separated  
48 domains [6, 7], substrate channeling of the metabolons [8], or long-distance interactions in  
49 DNA searching [9] and organization [10] have recently come to the forefront to question the  
50 discrepancy between the observed reaction rates in cells with the predictions of a strict random  
51 diffusion model [6, 11]. Within this framework, dipole-dipole electrodynamic interactions are  
52 predicted to promote molecular attraction by being selective through resonance and to act over  
53 long distances [12]. These forces can propagate without attenuation in electrolytes of ionic  
54 strength comparable to that in the cytoplasm, provided that their oscillation frequency exceeds  
55 the Maxwell frequency at few hundreds of MHz [13], since at such frequencies the Debye  
56 screening is ineffective [14]. Therefore, we hypothesize that, in addition to random diffusion,  
57 selective long-range attractive electrodynamic interactions increase the encounter rates between  
58 *A* and *B* cognate partners through a mutual force field described by a potential  $U(r)$  where  $r$  is  
59 the intermolecular distance. Then, after the Smoluchowski-Debye formula [15, 16], the associ-

60 ation rate is given by  $k_a^* = 4\pi R^*(D_A + D_B)$  where  $D_{A,B}$  are their diffusion coefficients and  $R^*$   
61 is given by

$$R^* = \left[ \int_{R_A+R_B}^{\infty} \frac{e^{U(r)/kT}}{r^2} dr \right]^{-1}. \quad (1)$$

62 where  $R_A, R_B$  are the hydrodynamic radii of  $A$  and  $B$ , respectively;  $k$  is the Boltzmann con-  
63 stant and  $T$  the temperature. Remarkably, for an attractive interaction,  $U(r) < 0$ , Equation (1)  
64 implies  $k_a^* > k_a = 4\pi(R_A + R_B)(D_A + D_B)$ , that is, an increase of the association rate with re-  
65 spect to the purely diffusive  $k_a$ . However, electrodynamic macromolecular interactions have not  
66 previously been considered for several reasons, including: *i*) they have never been observed in  
67 any experimental context, though theoretically predicted by both Classical [12, 17] and Quan-  
68 tum Electrodynamics [18]; *ii*) they require an out-of-equilibrium system [12], which though,  
69 of course, found in all living systems, is hard to organize in the laboratory *in vitro*, especially  
70 with molecules in metastable states with strongly excited giant dipole vibrations, as required for  
71 such interactions; *iii*) out-of-equilibrium collective vibrations of macromolecules are expected  
72 in the 0.1 – 1.0 THz domain, this is experimentally challenging to observe because of the strong  
73 absorption of water, and indeed such vibrations have only recently been detected for the first  
74 time [19] and corroborated by theoretical studies [20, 21]. Interestingly, the coherence of these  
75 collective molecular vibrations is theoretically expected to be long-lived [22].

76 Here we demonstrate experimentally the activation of long-range attractive electrodynamic  
77 forces between proteins. This was made possible through the study of R-Phycoerythrin (R-PE),  
78 a protein that can be excited naturally by an external energy supply, a light source. Then, by  
79 working at different concentrations (i.e. intermolecular distances) and excitation power of a  
80 laser as the light source, we have achieved what follows: *i*) observation of the activation of  
81 collective intramolecular oscillation of the proteins, a necessary pre-requisite to activate the  
82 physical mechanism pictorially outlined in Figure 1a; *ii*) observation of a distributed-clustering

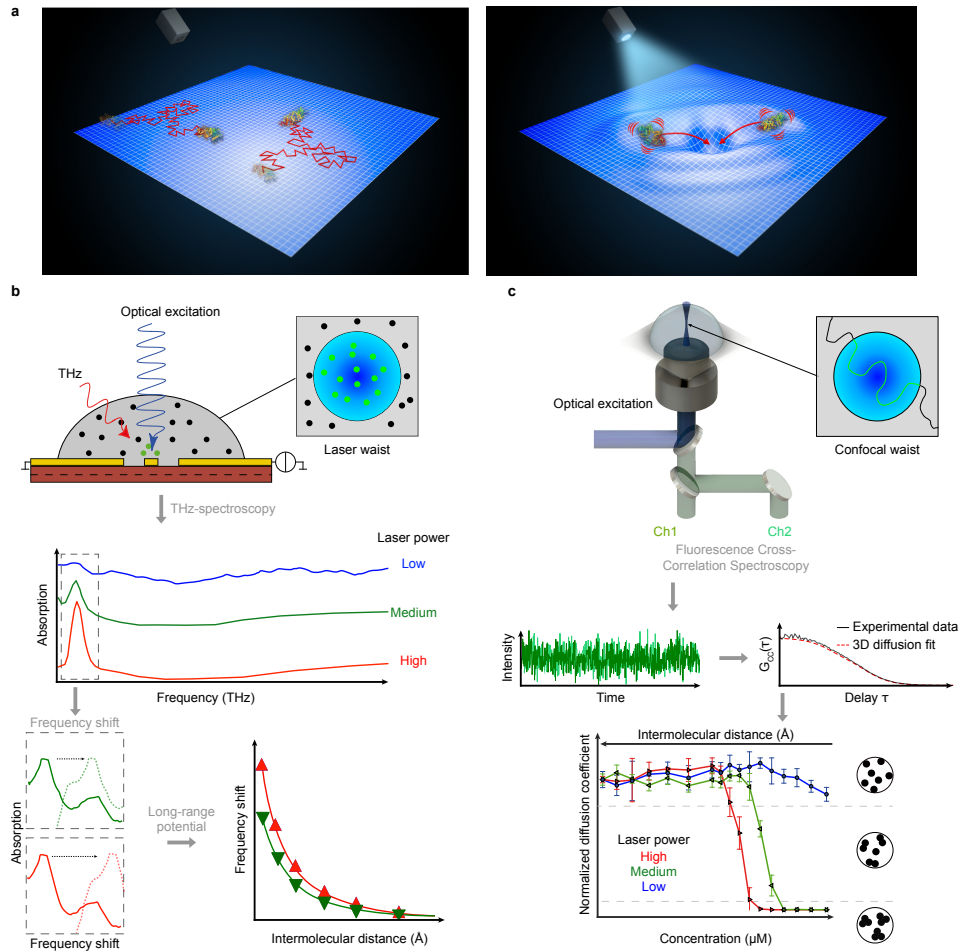


**Figure 1: Long-range electrodynamic interactions - Principle and experimental approaches** (a) At thermal equilibrium, macromolecules show a Brownian diffusive motion in solution (left panel). By switching-on an external energy source, molecules are in an out-of-thermal equilibrium collective vibrational state that can generate ED forces through associated large dipolar resonant oscillations (right panel). (b) In THz spectroscopy, the frequency of the collective vibration varies as a function of the average intermolecular distance (determined by the protein concentration). With respect to the reference frequency at "infinite" dilution, a frequency-shift inversely proportional to the cubic power of the average intermolecular distance is theoretically expected if the proteins interact through ED forces. (c) In FCS, the transit times of the proteins across the volume of observation are measured, hence the protein diffusion coefficients. Under out-of-thermal equilibrium conditions, the theory predicts a phase transition due to ED forces clustering proteins. This should be observed at a given protein concentration by a sudden drop in the diffusion coefficient from its Brownian value. In both (b) and (c), out-of-thermal equilibrium is activated by optical excitation.

83 transition dependent on activation of these collective molecular oscillations, as expected after a  
84 thorough preparatory work [3, 23, 24, 25], and *iii*) the consequent expected change of the fre-  
85 quency of the collective oscillation [26]. For this, two experimental techniques were used: THz  
86 spectroscopy, mainly composed of two setups using either a THz-rectenna or a microwire-probe  
87 as sensors, respectively (see Materials and Methods section for details), and fluorescence cor-  
88 relation spectroscopy (FCS) (Figure 1b,c). Overall, our experimental work supports a *proof-of-*  
89 *principle* that out-of-equilibrium collective oscillations are capable of activating dipole-dipole  
90 electrodynamic intermolecular forces, thus paving the way to explore the potential role of ED  
91 intermolecular forces in living matter.

## 92 **Results**

93 This first experimental study has been performed with a natural light-harvesting protein derived  
94 from red algae, the R-PE (see Figure S1 in [27]). This protein is an hexamer  $(\alpha\beta)_6\gamma$  where the  
95 subunit  $\alpha$  contains two phycoerythrobilins, the subunit  $\beta$  contains three phycoerythrobilins and  
96 one phycourobilin and the  $\gamma$  subunit contains two or three phycoerythrobilins and one or two  
97 phycourobilins. That is, some limited variability in the number of fluorochromes is possible and  
98 38 fluorochromes is considered a typical number. All these subunits form one of the brightest  
99 fluorescent dye (the entire protein) hitherto found. These pigments are highly sensitive to the  
100  $\lambda = 488$  nm light used in these experiments.

101 Thus, under suitable illumination conditions (detail in Materials and Methods) of the R-PE  
102 molecules in saline solution, each molecule can enter a coherent vibrational state (Figure 2)  
103 displaying similar phenomena to those reported for Bovine Serum Albumin (BSA) protein in  
104 [19]: the existence of a threshold for the energy input rate to activate the collective mode, and  
105 a saturation of the oscillation amplitude at high values of the energy input rate. Two collective  
106 oscillation frequencies for R-PE are found. One at 0.071 THz ( $= 2.4 \text{ cm}^{-1}$ ) and another at

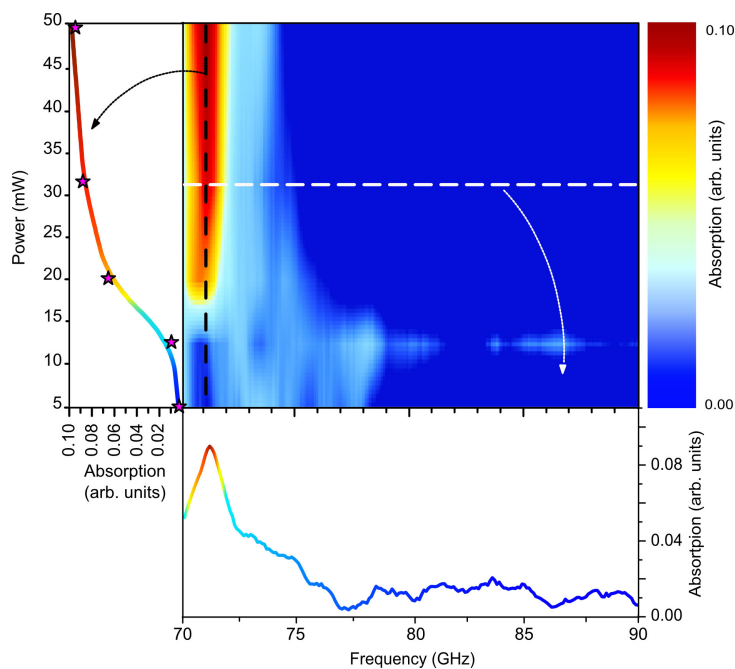


**Figure 2: Collective oscillation of the R-PE measured by THz-Spectroscopy.** Absorption strength of the R-PE (1 mg/mL in 200 mM NaCl) as a function of detection frequency and the laser power activating the molecular collective oscillation at a frequency of 71 GHz ( $2.4 \text{ cm}^{-1}$ ). The absorption line profile (bottom) indicated by the horizontal white dashed line was measured at an optical power of 31.5 mW, while the laser power threshold (left) behaviour is indicated by the black dashed line. Stars stand for experimental data and the interpolating line is just a guide to the eye.

107 0.096 THz ( $= 3.2 \text{ cm}^{-1}$ ) (see Figure 3). Even if a protein is not an idealized solid, or of strictly  
 108 well-defined shape, considering the best fitting simple geometric shape provided a successful  
 109 precedent with the BSA. The BSA is referred to as a globular protein and it is certainly not  
 110 a rigid, elastic, solid sphere, but by applying a formula for the spheroidal modes of an elastic  
 111 sphere an excellent agreement with the experimental finding was obtained [19]. Similarly, the  
 112 geometric shape that best fits the hexamer form of the R-PE is a torus. Even if such a treatment  
 113 of R-PE and BSA collective vibration modes is somewhat rudimentary, it provides information  
 114 adequate to what is needed in the present context. In fact, schematizing the R-PE protein as a  
 115 torus-shaped object of  $M = 240 \text{ kDalton}$ , with a larger midline radius  $R = 37.5 \text{ \AA}$ , a minor



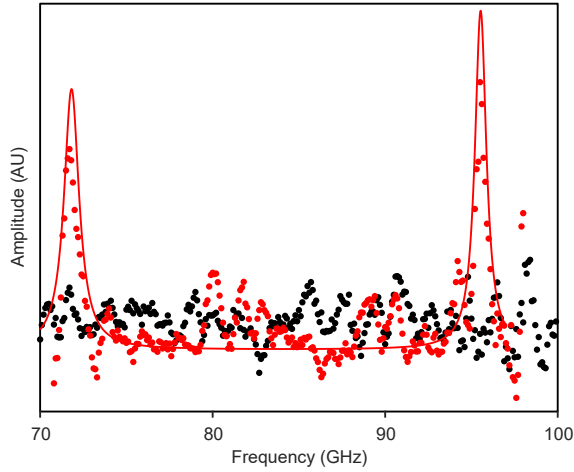


**Figure 3:** Comparison of the R-PE in saline solution (red) and saline solution without R-PE (black). Two collective extension modes of R-PE appear at 71 GHz and 96 GHz. Experimental data (full circles); Lorentz fit (solid line).

116 radius  $r = 30 \text{ \AA}$  [28], density  $\rho$  (the ratio between  $M$  and the volume of the torus), and Young  
 117 elastic modulus  $E$ , the frequencies of the collective extension modes (those corresponding to  
 118 oscillating larger radius  $R$ ) are given by [29]

$$\nu_n = \frac{(1 + n^2)^{1/2}}{2\pi R} \left( \frac{E}{\rho} \right)^{1/2}. \quad (2)$$

119 Hence the ratio  $\nu_1/\nu_0 = \sqrt{2} \simeq 1.41$  which approximates within a 4% the ratio between the  
 120 observed frequencies, that is  $0.096/0.071 = 1.35$ . The Young modulus of R-PE is not known  
 121 in the literature, but by inverting the above formula we obtain  $E \simeq 5.3 \text{ GPa}$  which seems  
 122 reasonable knowing that at 300 K for Myoglobin  $E \simeq 3.5 \text{ GPa}$ , and for BSA  $E \simeq 6.75 \text{ GPa}$   
 123 [30] (both proteins being mostly made of  $\alpha$ -helices like R-PE). Remarkably, such an empirical  
 124 approach gives a useful insight on the observed phenomenology as it was successfully done for  
 125 the BSA [19].

126 A theoretically expected signature of attractive electrodynamic forces among macromolecules  
 127 vibrating at the same frequency is a phase transition between a dispersed phase of rapidly diffus-  
 128 ing molecules, and a clustered phase of very slowly moving aggregates of molecules [24] (see

129 Supplementary Materials). The control parameter of this transition is the average intermolecular  
130 distance, which is set by adjusting the molecular concentration.

131 In the fluorescence correlation spectroscopy (FCS) experiments, the protein concentrations  
132  $\mathcal{C}$  have been varied in the interval between 0.1  $\mu\text{M}$  and 10  $\mu\text{M}$  to make the average intermolec-  
133 ular distance  $\langle r \rangle = \mathcal{C}^{-1/3}$  vary in the interval 550 – 1950  $\text{\AA}$ .

134 The ionic strength of the protein solution is kept at 200 mM by means of suitable concen-  
135 trations of NaCl in water. This ensures a good shielding of electrostatic interactions. Moreover,  
136 the laser power ( $\lambda = 488 \text{ nm}$ ) has been varied between 50 and 150  $\mu\text{W}$ . Typical fluorescence  
137 traces are reported for different laser powers and protein concentrations in [27] (Figures S4 and  
138 S5).

139 The diffusion times  $\tau_D$  determined from the Cross Correlation Functions (CCFs) of fluo-  
140 rescence traces, and the measured waist of the confocal volume where the molecules are both  
141 excited and observed, allow estimation of the diffusion coefficients  $D$ . The use of CCFs is  
142 motivated in sections Methods and in Additional Data by Figures S2 and S3 of Ref. [27]. The  
143 values of the diffusion coefficient  $D$  are normalized with respect to the Brownian values  $D_0$  of  
144 each data series recorded at a given laser power (Figure 4). At low laser power the measured  
145 value of  $D_0$  matches the expected theoretical one  $D_0 = k_B T / (6\pi\eta R_H)$ , with  $\eta$  the viscosity  
146 of the solution, and  $R_H$  the hydrodynamic radius of the protein. At laser power of 50  $\mu\text{W}$ , the  
147 observed values of  $D$  (blue circles) do not change with the intermolecular distance. The diffu-  
148 sion of the R-PE molecules is Brownian for all the concentrations considered. This means that  
149 the energy input rate is either below the threshold value required to excite molecular collective  
150 vibrations, or the intermolecular ED forces are very weak because of the small amplitude of  
151 the collective vibrations of the R-PE proteins. The mismatch between the laser power values  
152 mentioned in Figure 2 for THz experiments and those reported above for diffusion experiments  
153 is due to the different volumes illuminated (see Methods in [27]).

154 At higher laser power,  $100 \mu W$ , obviously and consistently with a thermal effect, the mea-  
155 sured value of  $D_0$  at low concentration is larger than in the preceding case. However it cannot  
156 explain, in the interval of inter-molecular distances  $700 - 750 \text{ \AA}$  (green triangles), the steep drop  
157 of  $D/D_0$  that correlates with the increase of the fluorescence fluctuations and a sudden increase  
158 of the diffusion time  $\tau_D$ .

159 At the highest laser power considered,  $150 \mu W$ , again the steep drop of  $D/D_0$  is observed  
160 but now in the interval of inter-molecular distances  $900 - 950 \text{ \AA}$  (red triangles). In both cases,  
161 the steep drop of  $D/D_0$  correlates with a strong increase of the fluorescence fluctuations and a  
162 sudden and huge increase by several orders of magnitude of the diffusion time  $\tau_D$ . The strong  
163 increase of the fluorescence fluctuations is shown in Figure S6 where, for instance, at an aver-  
164 age inter-molecular distance of  $600 \text{ \AA}$  the variance of the fluorescence fluctuations is more than  
165 five orders of magnitude larger than the same quantity measured at an average inter-molecular  
166 distance of  $1950 \text{ \AA}$ . Correspondingly, the diffusion times measured through the correlation func-  
167 tions that are reported in the right lower panel of Figure S7 are 4.9 seconds and  $4.8 \times 10^{-5}$   
168 seconds at an average inter-molecular distance of  $600 \text{ \AA}$  and of  $1950 \text{ \AA}$ , respectively.

169 The steep drop of  $D/D_0$  and the increased amplitude of fluorescence fluctuations are the  
170 observable effects of a clustering phase transition stemming from the competition between the  
171 electrodynamic intermolecular attractive forces and thermal fluctuations. This is confirmed the-  
172 oretically by a semi-analytical model (Figure 4b), by Molecular Dynamics simulations and by  
173 Monte Carlo computations (see Supplementary Materials [27]). Molecular dynamics simula-  
174 tions have been done in order to estimate the effect of long-range electrodynamic interactions  
175 on the self-diffusion coefficient  $D$  of a system of interacting molecules defined by

$$D = \lim_{t \rightarrow +\infty} \frac{\langle \|\Delta \mathbf{r}_i(t)\|^2 \rangle_i}{6t} \quad (3)$$

176 where  $\Delta \mathbf{r}_i(t)$  is the displacement at time  $t$  of the  $i$ -th molecule with respect to its initial position,

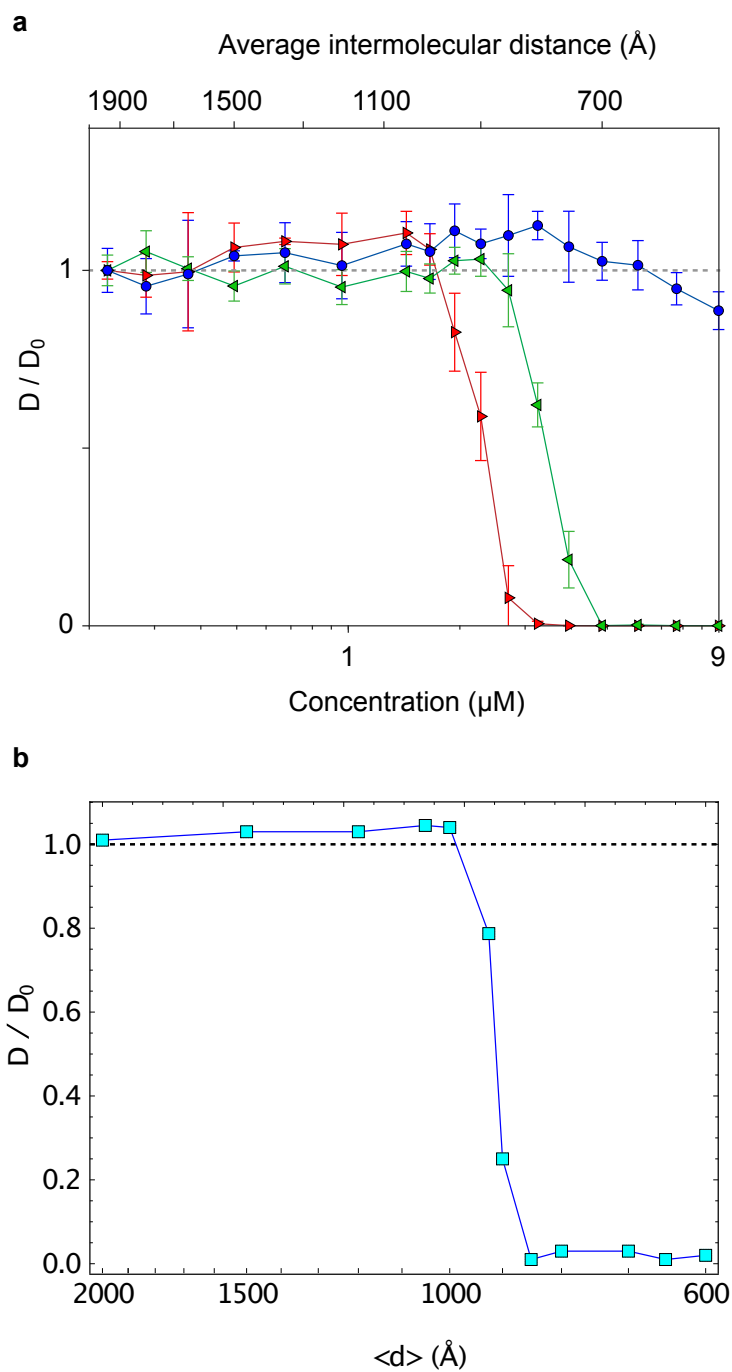


**Figure 4: Effect of protein concentration and laser power illumination on R-PE diffusion: Clustering phase transition.** (a) Diffusion coefficients normalized to the Brownian  $D_0$  values measured for each data series at  $0.223 \mu\text{M}$  ( $\langle r \rangle \simeq 1950 \text{ \AA}$ ) and recorded at  $50 \mu\text{W}$  (blue circles),  $100 \mu\text{W}$  (green triangles), and  $150 \mu\text{W}$  (red triangles). Each point corresponds to the average of 5 independent experiments. (b) Self-diffusion coefficient  $D/D_0$  (normalized to the Brownian value  $D_0$ ) versus intermolecular average distance  $\langle d \rangle$  for a system of particles in a cubic box interacting through long-range electrodynamic forces.

177 and  $\langle \cdot \rangle_i$  is the average over all the particles in the system. This is the physical quantity measured  
 178 by means of FCS experiments thus allowing a direct comparison between the outcomes of  
 179 numerical simulations and the outcomes of lab experiments.

180 The dynamics is described by the Langevin equations in the overdamped limit (without  
 181 inertial terms):

$$\frac{d\mathbf{r}_i}{dt} = -\frac{1}{\gamma} \nabla_{\mathbf{r}_i} \sum_{j \neq i} U(\|\mathbf{r}_i - \mathbf{r}_j\|) + \sqrt{\frac{2k_B T}{\gamma}} \boldsymbol{\xi}_i(t) \quad \forall i = 1, \dots, N \quad (4)$$

182 where  $\gamma$  is the viscous friction constant,  $U$  is the ED interaction potential,  $T$  is the temperature  
 183 of the solution and  $\boldsymbol{\xi}_i(s)$  is a noise term accounting for the random collisions of water molecules,  
 184 s.t.

$$\langle \xi_{A,i}(t) \rangle_t = 0 \quad \langle \xi_{A,i}(t) \xi_{B,j}(t') \rangle_t = \delta(t - t') \delta_{AB} \delta_{i,j} \quad \forall i, j = 1, \dots, N \quad \forall A, B = 1, \dots, 3 .$$

185 The parameters entering the model are chosen to reproduce the experimental conditions (details  
 186 are in Supplementary Material) and the sudden drop of the diffusion coefficient is found in cor-  
 187 respondence with the formation of clusters at an average intermolecular distance in agreement  
 188 with the experimental finding at  $150 \mu W$  in Figure 4a. In Figure 5 two snapshots are shown  
 189 of numerical Monte Carlo computations performed by considering long-range electrodynamic  
 190 interparticle forces. Thus, the appearance of clusters predicted theoretically has been experi-  
 191 mentally observed through the sudden enhancement of fluorescence fluctuation amplitudes and  
 192 long transit times across the confocal volume of the FCS setup. Clusters of R-PE were vi-  
 193 sually evidenced by fluorescence microscopy in Figure 6 and Video in online Supplementary  
 194 Materials.

195 Increasing the laser power, the higher the power the stronger the collective oscillation of  
 196 R-PE molecules and the larger the associated oscillating dipole moment. Hence the displace-  
 197 ment of the clustering transition to a greater average intermolecular distance for the stronger

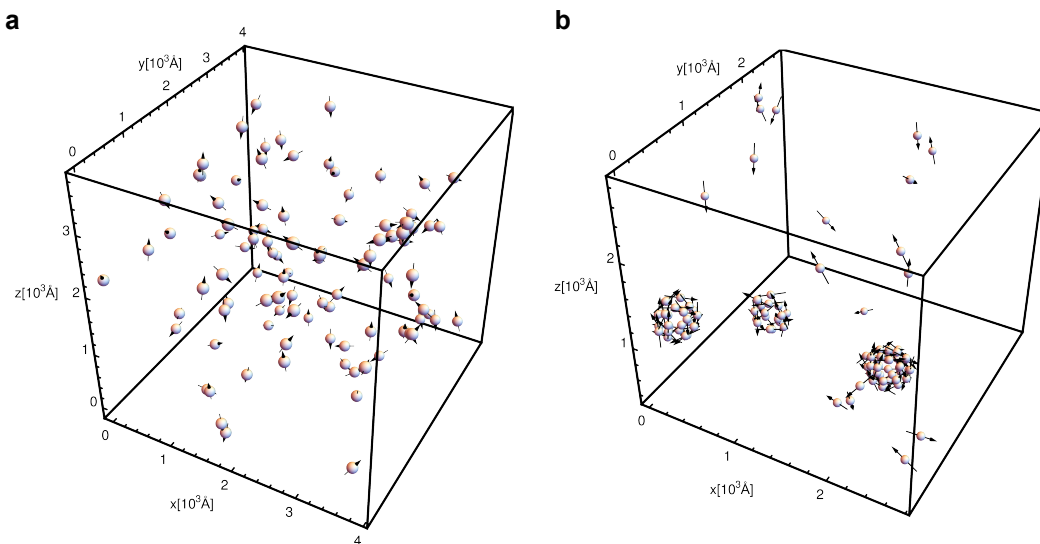


**Figure 5:** Snapshots of numerical Monte Carlo computations involving long-range electrodynamic inter-particle forces obtained with different initial values of  $\langle r \rangle$ . With  $\langle r \rangle_{initial} \simeq 1000 \text{ \AA}$  the system remains in the dispersed phase (lower left box) where  $D/D_0 = 1$  (Brownian diffusion); with  $\langle r \rangle_{initial} \simeq 950 \text{ \AA}$  the system switches to the clustered phase with  $D/D_0$  very small (lower right box).

198 molecular oscillations. Consistently, by suddenly lowering the power of the laser light supply  
 199 in the clustered phase a rapid disaggregation of the clusters is observed, as shown by the se-  
 200 quences of frames reported in Figure 6. Note that the frame on the left top of this figure shows  
 201 that, in the same conditions of temperature and particle concentration, when the energy input  
 202 rate is below the threshold value to activate intramolecular collective vibrations the clustering  
 203 transition disappears.

204 All these results are a clearcut proof of the activation of electrodynamic intermolecular  
 205 attractive forces due to the collective vibrations of the R-PE molecules. An independent con-  
 206 firmation of the activation of electrodynamic intermolecular attractive forces is obtained by  
 207 measuring the shift of the collective vibrational frequency as a function of the concentration  
 208 of molecules. Once again the proteins were observed in aqueous solution with the addition of  
 209 200 mM of NaCl to screen electrostatic interactions. In fact, theory predicts that electrody-

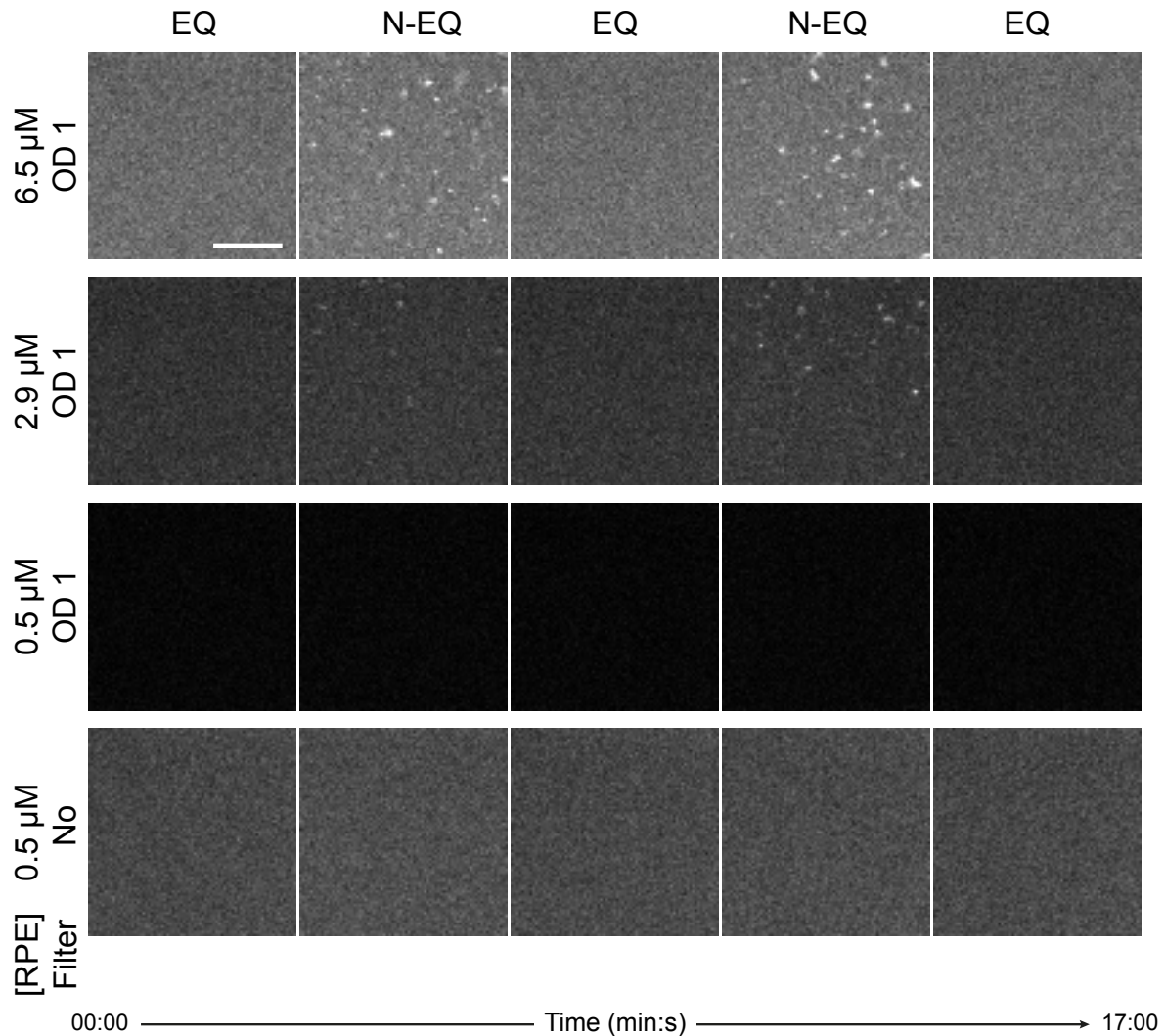


**Figure 6:** Screenshots saved out of a video of a solution of R-PE with optical power alternatively varying in time at  $50 \mu\text{W}$  and  $150 \mu\text{W}$ . EQ stands for proteins at equilibrium (switch-off of collective oscillations) and N-EQ for out of equilibrium (switch-on of collective oscillations). Snapshots have been taken for a concentration of  $0.5 \mu\text{M}$  (average molecular distance of  $\langle d \rangle = 1500 \text{ \AA}$ ) with and without optical density filter showing the absence of cluster formation at low concentration. At concentrations of  $2.9 \mu\text{M}$  ( $\langle d \rangle = 800 \text{ \AA}$ ) and  $6.5 \mu\text{M}$  ( $\langle d \rangle = 630 \text{ \AA}$ ) the formation of protein clusters and their reversibility are well evident. **The increase of the background brightness in the upper sequence of frames is due to the combined effects of the increase of protein concentration and of the laser power.** The scale bar corresponds to  $10 \mu\text{m}$ . The units of the time scale are expressed in min:sec.

210 namic dipole-dipole interaction between two molecules results in a shift  $\Delta\nu$  of their vibration  
211 frequency from the unperturbed frequency  $\nu_0$ , shift proportional to  $1/r^3$  with  $r$  the intermolec-  
212 ular distance [12]. Remarkably, this law is preserved also for a large number of interacting  
213 molecules, that is, the frequency shift is proportional to  $1/\langle r \rangle^3$  where  $\langle r \rangle$  is the average in-  
214 termolecular distance given by  $\langle r \rangle = C^{-1/3}$  (see Supplementary Materials for the theoretical  
215 explanation [27]). The unperturbed vibration frequency  $\nu_0$  is operationally measured at very  
216 low molecular concentration. The shifts  $\Delta\nu$  are then measured with respect to this value of  $\nu_0$ .  
217 The collective oscillation frequency of the R-PE at 0.071 THz (i.e.  $2.4 \text{ cm}^{-1}$ ) allowed to use as  
218 THz detector an electronic nano-device, namely a bow-tie antenna on the 2D electron gas layer  
219 of a FET transistor called a rectenna [31] (see Figure 8a of Materials and Methods section). The  
220 measured frequency shift is found to follow a linear dependence on the protein concentration,  
221 that is, the experimental outcomes are in excellent agreement with the theoretical predictions  
222 (Figure 7a). The steepening of the fitted lines in Figure 7a as laser power is increased is also in  
223 agreement with expectations. This is because the increasing oscillation amplitude (entailing a  
224 larger oscillating dipole moment), results in stronger intermolecular electrodynamic interaction  
225 and hence a larger frequency shift (for theoretical details see Supplementary Materials [27]).  
226 The case of R-PE is especially important because two independent experimental approaches  
227 lead to the same physical conclusion: the activation of intermolecular electrodynamic forces  
228 acting at a long distance. Thus the possibility of artefacts or misinterpretations is ruled out.  
229 Importantly, these forces are not peculiar of the R-PE since they are also observed by making  
230 measurements with another protein, BSA. BSA molecules were labeled with an average num-  
231 ber of 5 fluorochromes AF488 5-TFP, covalently bonded to the Lysine residues, excitable by  
232 the light emitted by a diode laser at 488 nm. The reason for considering the BSA is twofold:  
233 first, the labeled BSA molecules, when continuously supplied by laser light at  $\lambda = 488 \text{ nm}$ ,  
234 are driven in a collective vibration mode at 0.314 THz (i.e.  $10 \text{ cm}^{-1}$ ) [19]; second, R-PE and



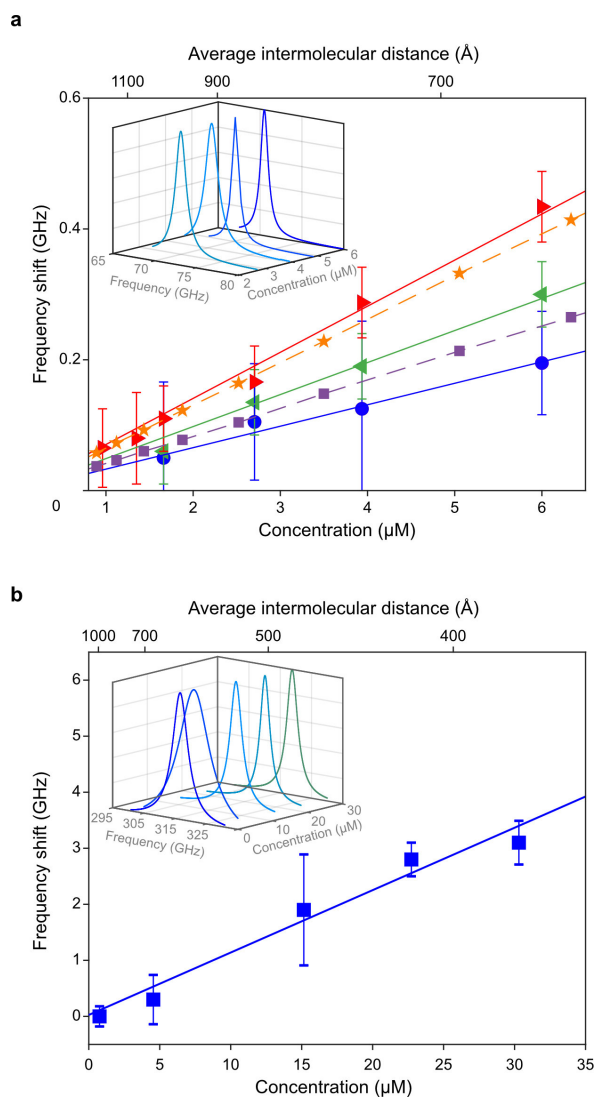


**Figure 7: Frequency shifts of the intramolecular collective vibrations of R-PE and BSA at different concentrations.** Measurements were performed at room temperature in aqueous solution with 200 mM of NaCl. Panel (a) refers to R-PE. The shift is relative to the reference frequency measured at the lowest protein concentration. Measurements have been performed at different powers of the laser: 31.5 mW (blue circles), 39.5 mW (green triangles), 50 mW (red triangles). Purple squares and orange stars refer to theoretical outcomes worked out with different values of molecular dipole moments (see Supplementary Materials). Panel (b) refers to BSA at a laser power of 40 mW. Insets: The frequency shifts are measured through a Lorentz fitting of the experimental resonances. The different colors in the insets are just a visual help.

235 BSA both have a structure composed largely of alpha-helices (Figure S1 in [27]), a property  
236 that we can suppose being facilitating the activation of collective vibrational modes. In fact,  
237 alpha-helices behave as springs undergoing the so-called accordion modes, therefore a protein  
238 mainly composed of alpha-helices is reasonably supposed to be highly flexible and its compo-  
239 nents can undergo synchronization phenomena possibly giving rise to a collective oscillation.  
240 The collective oscillation frequency of the BSA at 0.314 THz required the use of a near-field  
241 microwire-based probe coupled with a wave-guide (see Figure 8b of Materials and Methods  
242 section). Again, the measured frequency shift is found to follow a linear dependence on the  
243 protein concentration as expected (Figure 7b). This provides a remarkable confirmation of the  
244 activation of long distance electrodynamic interactions also for BSA.

245 It is worth pointing out that the two THz experimental setups have been operated at a differ-  
246 ent spatial density of the laser light, with respect to diffusion experiments, to prevent a clustering  
247 transition during the frequency shift measurements. In fact, by using a set of optical density fil-  
248 ters to lower the spatial density of the laser power, the ED forces can be weakened to the point  
249 of being unable to entail the clustering transition by overcoming thermal noise, and the protein  
250 molecules keep diffusing with a Brownian motion (see Materials and Methods section).

## 251 Discussion

252 In the work presented here, we have experimentally shown, for the first time, that the excitation  
253 of out-of-equilibrium collective oscillations is capable of driving molecular association through  
254 the activation of electrodynamic intermolecular forces. R-PE provides convincing evidence for  
255 these forces using a pair of complementary experimental approaches. Thus, R-PE represents the  
256 “*Rosetta stone*” allowing us to identify attractive intermolecular forces through two completely  
257 different physical effects.

258 Long-range electrodynamic interactions have also been activated using a second protein,

259 fluorescent dye-labeled BSA. These results confirm the generality of this phenomenon thus  
260 paving the way for the experimental searching of ED forces in the more complex environment  
261 encountered in cell biology.

262 A central feature of the ED forces activated by collective molecular vibrations is their long-  
263 range property, that is, they stem from an interaction potential decreasing as the third inverse  
264 power of the intermolecular distance. This generates first-order phase transitions with the for-  
265 mation of molecular condensates. A thorough theoretical analysis of this transitional behavior,  
266 and of the frequency shift of the collective vibrations of the proteins, caused by their interaction  
267 through ED forces, can be found in Supplementary Materials.

268 By being dynamic and reversible, ED forces can be instrumental in structuring the mesoscale  
269 molecular organization through the formation of biomolecular condensates and thus provide a  
270 rationale to explain the speed of many cellular processes. While we have evidence of the asso-  
271 ciation of biological macromolecules driven by ED forces *in vitro*, the conditions are far from  
272 the ones found *in cellulo*. Here, the energy sources necessary to maintain the molecules out-  
273 of-equilibrium need to be characterized. Among the potential candidates, there are: adenosine  
274 triphosphate (ATP) as a universal biological fuel, ionic currents such as those used to drive ATP  
275 synthesis, ionic collisions, photons produced by mitochondria, or external light [32, 33]. The  
276 notion of selectivity of ED forces will also need to be explored in a crowded environment com-  
277 posed of a vast diversity of molecular components. More specifically, it will be important to  
278 consider the possible role of ED forces between different molecular species (ligand-receptor,  
279 DNA-protein) co-resonating at one or more collective oscillation frequencies. [Interestingly,](#)  
280 [recent numerical studies have shown that correlations of electronic density fluctuations can ex-](#)  
281 [tends up to 30 Å in protein-solvent systems \[34\]. These correlations, responsible for long-range](#)  
282 [many-body van der Waals interactions, by structuring hydration layers, could support and give](#)  
283 [a contribution also to ED intermolecular interactions and communications among biomolecules.](#)

284 Moreover, our findings could be of general interest for methodological applications requir-  
285 ing a tight control in space and time of molecular interactions in living cells to decipher cellular  
286 functions. As an example, in the developing field of optogenetics where molecular interactions  
287 are switched on/off by engineered proteins controlled by light [35].

288 Further, ED forces could also be exploited in the domain of drug design. It has been hy-  
289 pothesized that combining steric complementarity with “long-range complementarity” could  
290 improve therapeutic efficiency. Thus, ED forces could allow recognition at a distance and drive  
291 an efficient mutual approach between a drug and its therapeutic target before their final chemical  
292 binding [36].

293 Finally, throughout evolution, life has exploited all the available physical laws, processes,  
294 and phenomena. It is thus exciting to speculate how the new phenomenon reported here for the  
295 first time has been used to gain adaptive advantage and possibly overcome some of the adverse  
296 effects of molecular crowding in cells.

## 297 **Materials and Methods**

### 298 **Theoretical rationale**

299 A crucial condition to activate long-range electrodynamic forces between biomolecules is to  
300 put them out-of-thermal-equilibrium, in a coherent vibrational state of all - or a large fraction  
301 - of their atoms. In fact, at thermal equilibrium a macromolecule “flickers”, that is, it under-  
302 goes incoherent and random deformations of all its subunits resulting in small noisy variations  
303 of its static dipole moment. At equilibrium, energy equipartition among the normal modes of  
304 vibration holds, thus the amplitude of collective modes is very small. Collective modes have  
305 been detected at equilibrium already a long time ago for proteins [37] and polynucleotides [38]  
306 with Raman and far infrared spectroscopy. But by keeping a macromolecule out of thermal  
307 equilibrium by means of an external energy supply a phonon condensation phenomenon can be

308 activated [19], consisting of the channelling of the supplied energy into a low frequency coher-  
309 ent mode of vibration of all the atoms (or of a significant fraction of them) of the same macro-  
310 molecule. So excited, the macromolecule may have a very large oscillating dipole moment. In  
311 turn, in such a collective oscillation state, a biomolecule could activate a long-range attractive  
312 electrodynamic interaction with other molecules if they possess a proper frequency close to that  
313 of the coherent mode. This scenario has been proposed a long time ago [39, 40, 41, 17] but  
314 has been marginalized for several reasons, including its quantum mechanical formulation and  
315 because it has never been given experimental evidence. Reformulated in a classical framework  
316 [12, 19], the above sketched scenario has been given new credit after the recent experimental  
317 proof of the possibility of activating a stationary oscillation of a macromolecule out of thermal  
318 equilibrium [19]. This is a necessary pre-condition to activate long-range electrodynamic inter-  
319 actions [12]. It is worth mentioning that in a recent work it has been convincingly maintained  
320 that a full understanding of Fröhlich condensation can come solely from a quantum theory [22].

## 321 **Theoretical design of the experiments**

322 A first method designed to detect long-range electrodynamic intermolecular forces is based on  
323 the expected change in the diffusion properties of the proteins at different concentrations, in the  
324 presence of both suitably activated electrodynamic forces and stochastic forces representing the  
325 random hits of water molecules on the proteins. The feasibility study of this approach has been  
326 carried out via theoretical computations resorting to Molecular Dynamics simulations. Exper-  
327 imentally, the FCS/FCCS methods that are based on recording the fluctuations of fluorescence  
328 signal in a small volume of observation (i.e., a confocal volume in FCS microscopy) have the  
329 sensitivity to infer information about the diffusion time through this volume [42]. The autocor-  
330 relation (cross-correlation) function of the detected fluorescence signal is fitted by means of an  
331 analytic formula derived by a theoretical model of diffusion. Hence the diffusion time  $\tau_D$ , that

332 corresponds to the average time molecules stay within the volume of observation, is obtained  
333 and the diffusion coefficient  $D$  is simply given by  $D = \omega_{xy}^2/4\tau_D$ , where  $\omega_{xy}^2$  is the lateral waist  
334 of the excitation beam focused through the objective of the microscope. This allows us to as-  
335 sess whether the transit time of fluorescent molecules follows a Brownian diffusion law (i.e.,  
336 resulting from stochastic forces generated by collisions with water molecules) or, instead, a law  
337 that possibly combines both electrodynamic forces and the stochastic forces just mentioned. A  
338 three steps feasibility study has validated this experimental strategy to detect these electrody-  
339 namic intermolecular forces [23, 24, 25]. In particular after the results reported in Ref.[24],  
340 the free Brownian diffusion was expected to be dramatically reduced by the formation of large  
341 molecular clusters when the concentration of the solvated molecules exceeds a critical value.  
342 These preliminary results have suggested to experimentally look for this hallmark of the activa-  
343 tion of electrodynamic interactions. However, a more advanced and thorough investigation of  
344 this clustering transition was in order, thus it has been done in the present work (see Section 2.3  
345 of the theoretical part of this Supplementary Material). By resorting to a semi-analytical model,  
346 to Molecular Dynamics simulations, and to Monte Carlo computations it is shown that the acti-  
347 vation of electrodynamic forces entails the existence of a first-order clustering phase transition.  
348 This transition between a "dispersed" phase and a "clustered" phase occurs at a critical value  
349 of the concentration of actively oscillating biomolecules out-of-thermal-equilibrium, therefore  
350 at a critical value of the average intermolecular distance. An independent and complementary  
351 experimental possibility of detecting the activation of intermolecular electrodynamic forces has  
352 been suggested in Ref.[12]. In that case, the frequency of the collective oscillation mode of an  
353 isolated macromolecule undergoes a shift when placed close to another macromolecule oscillat-  
354 ing at the same frequency. This shift is inversely proportional to the cube of the intermolecular  
355 distance. Remarkably, this remains true for a large number of molecules in solution (see Sec-  
356 tion 3 of the theoretical part of this Supplementary Material) in which case the frequency shift

357 is found again to be inversely proportional to the cube of the *average* intermolecular distance.  
358 If this represents an experimental crosscheck of the diffusion-based approach, challenge comes  
359 *a-priori* from the difficulty in implementing THz spectroscopic measurement of proteins in  
360 aqueous solutions due to the strong absorption of water in the THz and sub-THz frequency do-  
361 mains. But this difficulty is considerably reduced when measurements are performed under out-  
362 of-equilibrium conditions. In fact, this is distinct from standard spectroscopic measurements,  
363 where the incident radiation simultaneously excites the atoms or molecules under study and  
364 probes their absorption spectrum by sweeping a range of frequencies. With THz spectroscopy  
365 of out-of-equilibrium biomolecules in solution, the analysis is carried out on already active  
366 objects (whose vibrations are induced by an internal cascade or interconversion of light), and  
367 weak THz radiation is only used to read and detect active vibrations of the biomolecules. More-  
368 over, the absorption of THz radiation by the actively oscillating molecules is much stronger  
369 than the absorption of THz radiation by water, thus making molecular absorption features well  
370 detectable despite the presence of water.

### 371 **Two experiments operating in different conditions**

372 In the FCCS setup, the laser beam is focused in a small volume of about one femtoliter where a  
373 high energy density is attained. This is necessary to excite the collective oscillation of the R-PE  
374 molecules during their quick transit through the confocal volume of transversal diameter of 916  
375 nm. The R-PE molecules efficiently harvest light by means of their 38 fluorochromes within  
376 each protein molecule. On the contrary, in the THz spectroscopy setup, a much lower energy  
377 density was attained because the laser beam illuminated a large drop of solution of 35  $\mu\text{L}$ . This  
378 notwithstanding, the excitation of collective oscillations of both the BSA molecules and of the  
379 R-PE molecules, respectively, was attained - without making them cluster - by means of long  
380 exposure times. The activation of collective oscillations of the molecules in solution prevent-

381 ing at the same time their clustering (which simply means that the electrodynamic forces were  
382 unable to overcome the thermal forces) was a necessary condition, in fact, a clustered frac-  
383 tion of the molecules would have completely altered the relationship between frequency shift  
384 and concentration. This operating condition was obtained by adjusting the laser power so as  
385 to lower the threshold value of the average intermolecular distance of the clustering transition  
386 below  $500 \text{ \AA}$  for the R-PE. Moreover, the same laser power density was unable to induce the  
387 clustering phase transition of the BSA molecules because the power density was not enough  
388 to excite sufficiently strong collective oscillations. This is the reason why the BSA turned out  
389 not apt for the experiments based on self-diffusion. In fact, the BSA is not naturally sensi-  
390 tive to light, and, to get excited, its collective oscillation mode requires a very long time of  
391 light-pumping, via the artificially attached fluorochromes, of about 10 minutes [19] to make the  
392 corresponding absorption feature sharp enough. Long excitation times are necessary because,  
393 in our experimental conditions and for BSA, the rates of energy dissipation and energy input  
394 are almost equal. A long time is therefore needed to accumulate enough energy in each protein  
395 to make intra-molecular nonlinear interaction terms strong enough to activate the condensation  
396 phenomenon. For R-PE, which naturally absorbs light and contains a total of 38 fluorochromes,  
397 the process is much faster, and a time of less than three seconds is necessary to observe the  
398 formation of clusters in the FCS experiments, whereas in THz experiments about one minute is  
399 needed to begin to detect the spectral features corresponding to collective molecular vibrations  
400 and about 4 minutes are necessary to observe sharp absorption peaks. In both cases, the men-  
401 tioned values of time pumping is highly reproducible. Long illumination times were realised in  
402 the THz setup but this was not possible in the FCS/FCCS setups where the transit times through-  
403 out the confocal volume was exceedingly short to activate the collective oscillations of the BSA  
404 molecules in spite of the high light power density in the confocal volume. In conclusion, let us  
405 remark that the electrodynamic forces can be active also in the disperse phase when the proteins



406 undergo Brownian diffusion. In other words, even if these forces are not strong enough to make  
407 the clustering transition by winning against thermal disorder, they can nevertheless induce the  
408 frequency shifts reported in Figure 4.

## 409 **Biochemical samples**

410 R-PE was purchased from Merck (52412). BSA conjugated to Alexa Fluor<sup>TM</sup> 488 was pur-  
411 chased from Thermo Fischer Scientific (A13100). Samples were prepared by sequential dilu-  
412 tions of proteins in 200 mM NaCl. Their final concentrations were controlled by absorbance  
413 measurements (Nanodrop One Spectrophotometer, Thermo Fischer Scientific) at 566 nm for R-  
414 PE ( $\epsilon = 1\,960\,000\text{ M}^{-1}\text{cm}^{-1}$ ) and at 280 nm for BSA ( $\epsilon = 43824\text{ M}^{-1}\text{cm}^{-1}$ ) with a correction  
415 factor of 0.11 to account for AF488 at 280 nm.

## 416 **Fluorescence Correlation Spectroscopy experiments**

417 *Setup.* All fluorescence correlation spectroscopy measurements were performed on a confocal  
418 microscope (ALBA FCSTM, from ISS Inc., Champaign, USA) with a picosecond/CW 488 nm  
419 diode laser (BDL-488-SMN, Becker and Hickl, Germany) used at 80 MHz and focused through  
420 a water immersion objective (CFI Apo Lambda S 40X/1.25 WI, Nikon). The fluorescence  
421 collected by the same objective is split into two paths by a 50/50 beam splitter (Chroma 21000)  
422 and filtered by 525/40 nm band pass (Semrock FF02-525/40) before being detected by avalanche  
423 photodiodes (SPCM AQRH series, Perkin Elmer/Excelitas). Signals are recorded by a multitaу  
424 hardware correlator (FLEX-02-12D, Correlator.com, Bridgewater, NJ).

425 *Data acquisition.* Before each experiment, the laser power is adjusted at the back-aperture  
426 objective and, the lateral waist value  $\omega$  calculated knowing the diffusion coefficient of AF488  
427 [ $D_{AF488}(20^\circ\text{C}) = 409\text{ }\mu\text{m}^2/\text{s}$  derived from [43]] in aqueous solution at  $20^\circ\text{C}$  and according  
428 to the equation  $\omega^2 = 4D\tau_D$ . FFS measurements were performed on sample in 8-well LAB-

429 TEK chambers (Thermo Scientific Nunc) at given concentration of proteins diluted in 200 mM  
 430 NaCl. Five independent experiments were conducted for each condition (protein concentration  
 431 and laser power) with each individual measure corresponding to a series of 10 measurements  
 432 lasting 60 seconds. Different strategies have been previously applied to perform FCS measure-  
 433 ments at micromolar concentrations [44, 45]. Here, to overcome this concentration limitation,  
 434 which is mainly due to the detector limits, the collected signal was attenuated by optical density  
 435 (OD) filters on the path just after the emission filters. The addition of OD1 or OD1.3 filters  
 436 with transmission values of 10% and 5%, respectively, allows keeping records with satisfactory  
 437 amplitude fluctuations and count rates per molecule for reliable analyses. The effectiveness of  
 438 this experimental approach has been validated with high concentrations of aqueous solutions of  
 439 the Atto488 dye (Additional Data Figures S2 and S3). In addition, the use of the FCCS data  
 440 acquisition modality avoids post-pulse artefacts due to spurious photon detection [46].

441 **Data analysis.** As mentioned above, all data were collected in a FCCS mode for proper ex-  
 442 perimental analyses. Consequently, we analyze the fluctuations by a cross-correlation function  
 443 (CCF) defined as

$$G(\tau) = \frac{\langle \delta F_1(t) \delta F_2(t + \tau) \rangle}{\langle F_1 \rangle \langle F_2 \rangle}, \quad (5)$$

444 with  $\delta F_1(t)$  and  $\delta F_2(t)$  the signal collected by detector 1 and 2, respectively. The averages are  
 445 performed over time. We kept simplest the mathematical model fitting the CCF by using the  
 446 standard analytic form of the function  $G(\tau)$  for a one-component system in a 3D environment  
 447 which reads as [47]

$$G(\tau) = \frac{1}{N} \left( \frac{1}{(1 + \tau/\tau_D) \sqrt{1 + s^2 \tau/\tau_D}} \right), \quad (6)$$

448 where  $N$  is the average number of molecules,  $\tau_D$  the average diffusion time of the tracer through  
 449 the confocal volume, and  $s$  the structure parameter of the confocal volume, that is, its axial to  
 450 lateral waist ratio  $\omega_{xy}/\omega_z$ . Still, the fitting accuracy of CCFs with Eq.(6) is no longer very good  
 451 with high laser power and at high concentrations (Additional Data Figure S7) because of CCF

452 distortion due to very long transit times of protein clusters. Therefore, the CCFs that are no  
453 longer accurately fitted by the standard function  $G(\tau)$  are preliminarily smoothed by applying a  
454 Savitzky-Golay filter using a polynomial of third degree (red curves on Additional Data Figure  
455 S7). This allows to get reasonable estimates of  $\tau_D$  as the lag time corresponding to the half-  
456 height of the smoothed CCF. Note that when the R-PE concentration exceeds even slightly a  
457 clustering critical value, these estimates are fully acceptable and adequate for our purposes.  
458 In fact, in this case  $\tau_D$  suddenly increases of several orders of magnitude with respect to its  
459 Brownian value, thus making the details of its estimation irrelevant. The variation of  $\tau_D$  is also  
460 so large that the effects of the high level of noise at short lag-times on its estimate do not have  
461 any meaningful consequence on the clear evidence of the clustering phase transition.

## 462 **Confocal video-microscopy**

463 The confocal video-microscopy images were performed on a confocal microscope (ALBA FC-  
464 STM, from ISS Inc., Champaign, USA) with a picosecond/CW 488 nm diode laser (BDL-488-  
465 SMN, Becker and Hickl, Germany) used at 80 MHz and focused through a water immersion  
466 objective (CFI Apo Lambda S 40X/1.25 WI, Nikon). The fluorescence collected by the same  
467 objective is filtered by a 525/40 nm band pass (Semrock FF02-525/40) before being detected by  
468 avalanche photodiodes (SPCM AQRH series, Perkin Elmer/Excelitas). Each  $128 \times 128$  pixel  
469 confocal image correspond to a  $30 \times 30 \mu\text{m}$  field of view and recorded at a pixel dwell time of  
470 0.1 ms at a rate of 2.8 s/frame.

## 471 **Captions for Movies S1 - S4**

472 **Mov1-seq1-v1** : R-PE protein concentration 0.5 micro Moles (absence of protein clusters). No  
473 optical filter. Each  $128 \times 128$  pixel confocal image corresponds to a  $30 \times 30 \mu\text{m}$  field of view  
474 and recorded at a pixel dwell time of 0.1 ms at a rate of 2.8 s/frame. Each stack of images was

475 made of 375 images where the laser power has been adjusted every 75 images to 50, 150, 50,  
476 150 and then 50  $\mu$ W. When indicated, an OD1 filter (Thorlabs ND-10B) has been added before  
477 the detector. Then, the video made from these images were compressed at a rate of 7 frame/s.  
478 Thus, each second of video corresponds to about 21 seconds of measurements.

479 **Mov2-seq2-v1** : R-PE protein concentration 0.5 micro Moles (absence of protein clusters).  
480 Each 128 x 128 pixel confocal image correspond to a 30 x 30  $\mu$ m field of view and recorded  
481 at a pixel dwell time of 0.1 ms at a rate of 2.8 s/frame. Each stack of images was made of 375  
482 images where the laser power has been adjusted every 75 images to 50, 150, 50, 150 and then  
483 50  $\mu$ W. An OD1 filter (Thorlabs ND-10B) has been added before the detector. Then, the video  
484 made from these images were compressed at a rate of 7 frame/s. Thus, each second of video  
485 corresponds to about 21 seconds of measurements.

486 **Mov3-seq3-v1** : R-PE protein concentration of 2.9 micro Moles (protein clusters are observed).  
487 Each 128 x 128 pixel confocal image correspond to a 30 x 30  $\mu$ m field of view and recorded  
488 at a pixel dwell time of 0.1 ms at a rate of 2.8 s/frame. Each stack of images was made of 375  
489 images where the laser power has been adjusted every 75 images to 50, 150, 50, 150 and then  
490 50  $\mu$ W. An OD1 filter (Thorlabs ND-10B) has been added before the detector. Then, the video  
491 made from these images were compressed at a rate of 7 frame/s. Thus, each second of video  
492 corresponds to about 21 seconds of measurements.

493 **Mov4-seq4-v1** : R-PE protein concentration 6.5 micro Moles (protein clusters are observed).  
494 Each 128 x 128 pixel confocal image correspond to a 30 x 30  $\mu$ m field of view and recorded  
495 at a pixel dwell time of 0.1 ms at a rate of 2.8 s/frame. Each stack of images was made of 375  
496 images where the laser power has been adjusted every 75 images to 50, 150, 50, 150 and then  
497 50  $\mu$ W. An OD1 filter (Thorlabs ND-10B) has been added before the detector. Then, the video  
498 made from these images were compressed at a rate of 7 frame/s. Thus, each second of video  
499 corresponds to about 21 seconds of measurements.

## 500 **THz spectroscopy experiments**

501 Long-range interactions between macromolecules can be highlighted through the dependence  
502 of their collective oscillation frequency, lying within the THz domain, on intermolecular dis-  
503 tance or concentration. THz near-field spectroscopy allows to measure the occurrence of such  
504 collective oscillations if one is able to realize this spectroscopy on proteins immersed in saline  
505 solution: a well-known technological roadblock, due to the huge absorption of THz radiations  
506 by water. We thus have developed two specific setups to overcome this limitation operating in  
507 the 0.07-0.11 THz domain and in the 0.25-0.37 THz range, respectively.

### 508 ***1. Rectenna-based THz-spectroscopy.***

509 **Setup.** For the 0.07 to 0.11 THz band, a continuous-wave (CW) THz radiation was generated  
510 by a Virginia Diodes WR10 source with 25 mW output power. A droplet of 30 - 35  $\mu\text{L}$  of  
511 a solution of R-PE (see Methods) was filed into a 14-pin ceramic dual in-line package (DIL)  
512 forming a cuvette where the rectenna (a bow-tie antenna connected to a GaAs/AlGaAs high-  
513 electron-mobility transistor) is placed (Figure 8(a)). A plastic-(transparent to blue and THz  
514 radiations) film was used to seal the system and to reduce evaporation. To excite the proteins,  
515 a Spectra Physics<sup>TM</sup> blue laser (ExcelsiorOne 488C-50) emitting at 488 nm and delivering a  
516 maximum of 50 mW (considering a 1 mm beam-diameter, with an optical-power density of  
517  $\approx 6.4 \text{ W cm}^{-2}$ ) was collimated onto the detector by using a dielectric plane-mirror. The laser  
518 output-power is controlled by a set of optical-density filters.

519 **Data acquisition.** THz passing through the solution of water, NaCl and excited protein  
520 is detected by the rectenna providing a DC-voltage at its loads, proportional to the THz-field  
521 intensity. While the dimensions of the rectenna reach half-a-wavelength (at 0.3 THz), the THz-  
522 field is only enhanced in the feed-gap region of the antenna e.g. within a volume of about 0.2  
523 pL. A hydrophobic, biocompatible and transparent to both THz and blue radiations varnish was  
524 applied to the upper layer of the rectenna. Experiments were done at room temperature.

525 **Data analysis.** Normalization procedure, according to Beer–Lambert law, divides spectra  
 526 of proteins in solution under illumination  $I_{R-PEON}$  by spectra of proteins in solution without  
 527 illumination  $I_{R-PEOFF}$ . To obtain spectra of excited proteins only –  $A$  is thus proportional to  
 528 the absorbance coefficient of excited proteins – the result is then divided by the buffer spectra  
 529  $I_{NaCl}$  (also with and without illumination).

$$A = \log \left( \frac{I_{R-PEON} \div I_{R-PEOFF}}{I_{NaClON} \div I_{NaClOFF}} \right). \quad (7)$$

530 Savitsky – Golay smoothing was used at the end to smooth curves, with 15 points of window  
 531 and a polynomial order of 2 (see an example of data treatment in Supplementary Material Figure  
 532 S9 [27]).

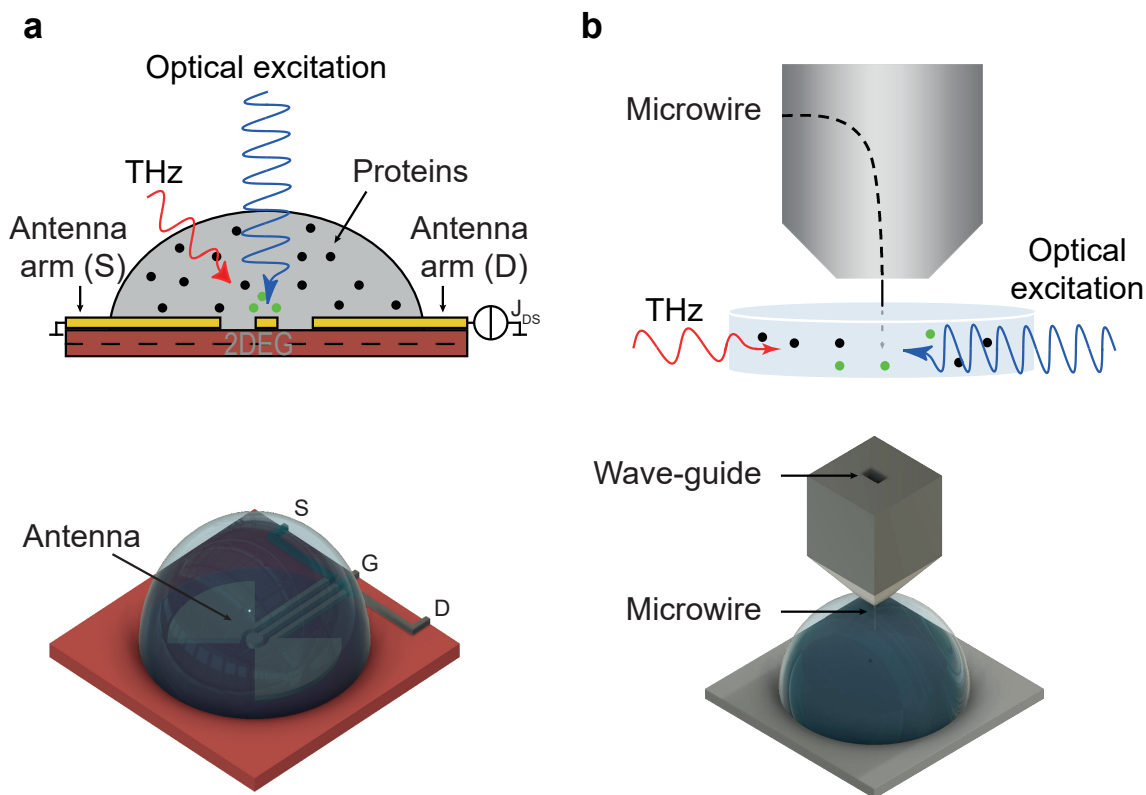


**Figure 8:** THz-spectroscopy experimental setups. (a) Rectenna for the 0.07 to 0.11 THz band; (b) Microwire-based probe for the 0.25 to 0.37 THz band.

## 533 *2. Microwire-based probe.*

534 **Setup.** For the 0.25 to 0.37 THz band, CW-THz radiation is produced by a Signal Generator  
535 Extension (SGX) module designed by Virginia Diodes, Inc. Module WR9.0 (82-125 GHz)  
536 SGX was used with external multiplier WR2.8 to extend the frequency coverage to 0.25-0.37  
537 THz with an average power of 1 mW. The radiation emitted is then collimated and focused by  
538 PTFE lenses on the biological sample. Optical excitation, represented by a blue laser and a UV  
539 lamp, was used to excite different components of the protein under study. Thus, for the optical  
540 excitation of fluorochromes, a Cobolt 06-MLD laser was used emitting an output-power of 40  
541 mW at the wavelength of 488 nm. Optical excitation of aromatic amino acids included in the  
542 protein was performed using LED M275L4 produced by ThorLabs at a wavelength of 275 nm  
543 and a typical output-power of 60 mW. Due to its large numerical aperture (NA=0.86) UV-coated  
544 lenses were used to collimate and focus the radiation onto the sample. Thus, a spot size of about  
545 1cm in diameter was achieved. A micro-coaxial near-field wire (Figure S8(b)) is inserted inside  
546 a metallic rectangular waveguide to allow a modal transition from TM<sub>01</sub> Sommerfeld's mode  
547 to TE<sub>01</sub> waveguide mode. The probe is capable of highly localized detection of the longitudinal  
548 component of the electric field [48] due to the sub-wave diameter of the wire around 10  $\mu\text{m}$  at  
549 the tip into the volume of about 4 pL.

550 **Data acquisition.** A specific sample holder was also designed. It is constituted by a plastic  
551 cylinder, transparent to UV, blue and THz radiations and resistant to UV radiation with a diam-  
552 eter of 7 mm and a volume of 53  $\mu\text{L}$ . At its bottom, a 130  $\mu\text{m}$ -thick glass was used, through  
553 which laser excitation was performed. To avoid evaporation and, as a consequence, changes in  
554 protein concentration during the experiment, the sample was covered by a plastic film with a  
555 thickness of 5  $\mu\text{m}$ , allowing the wire to pass through it without damage.

556 **Data analysis.** Regarding the normalization, the same procedure than in rectenna experi-  
557 ments has been followed, according to Beer–Lambert law, to obtain spectra of excited proteins

558 only. However, since in this frequency-band (0.25 - 0.37 THz) the signal-to-noise ratio is poor  
559 due to high absorption by water molecules, a specific data processing and normalization pro-  
560 cedure (using a band-stop Fourier transform filtering and Lorentz functions fitting) has been  
561 followed to extract an usable signal and frequencies of collective-oscillation resonances.

562 It is thus possible to observe the evolution of the absorption-peak amplitude as a function  
563 of the duration of illumination. Were considered as absorption peaks, those whose height and  
564 area are increasing continuously with time. Time (up to 1 hour) and concentration (from 750 to  
565 60,000 nM) dependences of the THz-spectra have been characterized.

## 566 **References**

- 567 [1] Venkatesan, K. & et al. An empirical framework for binary interactome mapping. *Nature*  
568 *Methods* **6**, 83 – 90 (2009).
- 569 [2] Bonetta, L. Interactome under construction. *Nature* **468**, 851–852 (2010).
- 570 [3] Gori, M., Donato, I., Floriani, E., Nardecchia, I. & Pettini, M. Random walk of passive  
571 tracers among randomly moving obstacles. *Theoretical Biology and Medical Modelling*  
572 **13**, 13–33 (2016).
- 573 [4] Banks, D. S. & Fradin, C. Anomalous diffusion of proteins due to molecular crowding.  
574 *Biophysical Journal* **89**, 2960 – 2971 (2005).
- 575 [5] Golan, Y. & Sherman, E. Resolving mixed mechanisms of protein subdiffusion at the T  
576 cell plasma membrane. *Nature Commun* **8**, 15851–15866 (2017).
- 577 [6] Banani, S., Lee, H., Hyman, A. & Rosen, M. Biomolecular condensates: organizers of  
578 cellular biochemistry. *Nature Rev. Mol. Cell Biol.* **18**, 285 – 298 (2017).



- 579 [7] Berry, J., Brangwynne, C. P. & Haataja, M. Physical principles of intracellular organiza-  
580 tion via active and passive phase transitions. *Reports on Progress in Physics* **81**, 046601 –  
581 046643 (2018).
- 582 [8] Sweetlove, L. J. & Fernie, A. R. The role of dynamic enzyme assemblies and substrate  
583 channelling in metabolic regulation. *Nature Communications* **9**, 2136 – 2148 (2018).
- 584 [9] Kulaeva, O. I., Nizovtseva, E. V., Polikanov, Y. S., Ulianov, S. V. & Studitsky, V. M. Dis-  
585 tant activation of transcription: Mechanisms of enhancer action. *Molecular and Cellular*  
586 *Biology* **32**, 4892 – 4897 (2012).
- 587 [10] Wang, J. *et al.* Exploring the mechanisms of genome-wide long-range interactions: inter-  
588 preting chromosome organization. *Briefings in Functional Genomics* **15**, 385–395 (2016).
- 589 [11] Wheeldon, I., Minter, S., Banta, S. & et al. Substrate channelling as an approach to  
590 cascade reactions. *Nature Chemistry* **8**, 299 – 309 (2016).
- 591 [12] Preto, J., Pettini, M. & Tuszynski, J. A. Possible role of electrodynamic interactions in  
592 long-distance biomolecular recognition. *Phys. Rev. E* **91**, 052710–052728 (2015).
- 593 [13] de Xammar Oro, J. R., Ruderman, G. & Grigera, J. R. Electrostatics of interactions  
594 in electrolyte media. possible consequences in biological functions. *Biophysics* **53**, 195 –  
595 198 (2008).
- 596 [14] Maxwell, J. C. *A Treatise on Electricity & Magnetism* (Dover Publications Inc., New-  
597 York, 1954).
- 598 [15] Debye, P. Reaction rates in ionic solutions. *Transactions of The Electrochemical Society*  
599 **82**, 265 – 272 (1942).

- 600 [16] Noyes, R. M. Effects of diffusion rates on chemical kinetics. *Prog. React. Kinet.* **1**, 129  
601 (1961).
- 602 [17] Fröhlich, H. Long-range coherence in biological systems. *Rivista Nuovo Cimento* **7**, 399  
603 – 418 (1977).
- 604 [18] Salam, A. *Molecular Quantum Electrodynamics* (John Wiley and Sons, Inc., New Jersey,  
605 2010).
- 606 [19] Nardecchia, I., Torres, J., Sturgis, J., Pettini, M. & et al. Out-of-equilibrium collective  
607 oscillation as phonon condensation in a model protein. *Phys. Rev. X* **8**, 031061 – 031084  
608 (2018).
- 609 [20] Kurian, P., Dunston, G. & Lindsayk, J. How quantum entanglement in DNA synchro-  
610 nizes double-strand breakage by type ii restriction endonucleases. *Journal of Theoretical*  
611 *Biology* **391**, 102–112 (2016).
- 612 [21] Kurian, P., Capolupo, A., Craddock, T. & Vitiello, G. Water-mediated correlations in  
613 DNA-enzyme interactions. *Physics Letters A* **382**, 33 – 43 (2018).
- 614 [22] Zhang, Z., Agarwal, G. S. & Scully, M. O. Quantum fluctuations in the fröhlich condensate  
615 of molecular vibrations driven far from equilibrium. *Physical Review Letters* **122**, 158101–  
616 158107 (2019).
- 617 [23] Preto, J., Floriani, E., Nardecchia, I., Ferrier, P. & Pettini, M. Experimental assessment of  
618 the contribution of electrodynamic interactions to long-distance recruitment of biomolec-  
619 ular partners: Theoretical basis. *Phys. Rev. E* **85**, 041904 – 041916 (2012).

- 620 [24] Nardecchia, I., Gori, M., Floriani, E., Pettini, M. & et al. Experimental detection of long-  
621 distance interactions between biomolecules through their diffusion behavior: Numerical  
622 study. *Phys. Rev. E* **90**, 022703 – 022717 (2014).
- 623 [25] Nardecchia, I., Lechelon, M., Gori, M., Pettini, M. & et al. Detection of long-range  
624 electrostatic interactions between charged molecules by means of fluorescence correlation  
625 spectroscopy. *Phys. Rev. E* **96**, 022403 – 022416 (2017).
- 626 [26] Olmi, S., Gori, M., Donato, I. & Pettini, M. Collective behavior of oscillating electric  
627 dipoles. *Scientific Reports* **8**, 15748 – 15760 (2018).
- 628 [27] See supplementary materials on science online. URL [supplementary materials](#).
- 629 [28] Chan, W.-r. & et al. Crystal structure of r-phycoerythrin from polysiphonia urceolata at  
630 2.8 Å resolution. *Journal Molecular Biology* **262**, 721 – 731 (1996).
- 631 [29] Blevins, R. D. *Formulas for natural frequency and mode shape* (Van Nostrand Reinhold  
632 Company, New-York, 1979).
- 633 [30] Perticaroli, S. *et al.* Secondary structure and rigidity in model proteins. *Soft Matter* **9**,  
634 9548–9556 (2013).
- 635 [31] Schuster, F. *et al.* Broadband terahertz imaging with highly sensitive silicon CMOS-  
636 detectors. *Opt. Express* **19**, 7827 – 7832 (2011).
- 637 [32] Van Wijk, R. *et al.* Integrating ultra-weak photon emission analysis in mitochondrial  
638 research. *Frontiers in Physiology* **11**, 717 (2020).
- 639 [33] Celardo, G. L., Angeli, M., Craddock, T. J. A. & Kurian, P. On the existence of superra-  
640 diant excitonic states in microtubules. *New Journal of Physics* **21**, 023005 (2019).

- 641 [34] Stöhr, M. & Tkatchenko, A. Quantum mechanics of proteins in explicit water: The role  
642 of plasmon-like solute-solvent interactions. *Science Advances* **5**, eaax0024 (2019).
- 643 [35] Tischer, D. & Weiner, O. D. Illuminating cell signalling with optogenetic tools. *Nature*  
644 *Rev. Mol. Cell Bio.* **15**, 551 – 558 (2014).
- 645 [36] Veljkovic, N., Glisic, S., Perovic, V. & Veljkovic, V. The role of long-range intermolecular  
646 interactions in discovery of new drugs. *Expert Opinion Drug Discovery* **6**, 1263–1270  
647 (2011).
- 648 [37] Painter, P., Mosher, L. & Rhoads, C. Low-frequency modes in the raman spectra of pro-  
649 teins. *Biopolymers* **21**, 1469–1472 (1982).
- 650 [38] Painter, P. C., Mosher, L. & Rhoads, C. Low-frequency modes in the raman spectrum of  
651 DNA. *Biopolymers* **20**, 243–247 (1981).
- 652 [39] Fröhlich, H. Long-range coherence and energy storage in biological systems. *Interna-*  
653 *tional Journal of Quantum Chemistry* **2**, 641– 649 (1968).
- 654 [40] Fröhlich, H. Long range coherence and the action of enzymes. *Nature* **228**, 1093 (1970).
- 655 [41] Fröhlich, H. Selective long range dispersion forces between large systems. *Physics Letters*  
656 *A* **39**, 153–154 (1972).
- 657 [42] Haustein, E. & Schwille, P. Fluorescence correlation spectroscopy: Novel variations of  
658 an established technique. *Annual Review of Biophysics and Biomolecular Structure* **36**,  
659 151–169 (2007). PMID: 17477838.
- 660 [43] Petrášek, Z. & Schwille, P. Precise measurement of diffusion coefficients using scanning  
661 fluorescence correlation spectroscopy. *Biophysical Journal* **94**, 1437–1448 (2008).

- 662 [44] Laurence, T. & et al. Fluorescence correlation spectroscopy at micro-molar concentra-  
663 tions without optical nanoconfinement. *Journal of Physical Chemistry* **B118**, 9662 – 9667  
664 (2014).
- 665 [45] Khatua, S. & et al. Enhanced-fluorescence correlation spectroscopy at micro-molar dye  
666 concentrations around a single gold nanorod. *Physical Chemistry Chemical Physics* **17**,  
667 21127 – 21132 (2015).
- 668 [46] Zhao, M. *et al.* Afterpulsing and its correction in fluorescence correlation spectroscopy  
669 experiments. *Applied Optics* **42**, 4031 – 4036 (2003).
- 670 [47] Magde, D., Elson, E., Hyman, A. & Webb, W. Fluorescence correlation spectroscopy. ii.  
671 an experimental realization. *Biopolymers* **13**, 29 – 61 (1974).
- 672 [48] Keilmann, F. Fir microscopy. *Infrared Phys. Techno.* **36**, 217–224 (1995).

## 673 **Acknowledgements**

674 The project leading to this publication has received funding from the Excellence Initiative  
675 of Aix-Marseille University - A\*MIDEX, a French "Investissements d'Avenir" programme.  
676 This work was also partially supported by the Seventh Framework Programme for Research  
677 of the European Commission under FET-Proactive grant TOPDRIM (FP7-ICT-318121), by the  
678 projects SIDERANT and NEBULA financed by the french CNRS, by the Occitanie Region  
679 and by Montpellier University through its TOP platform and by the LabEx NUMEV (ANR-  
680 10-LABX-0020) within the I-Site MUSE. We acknowledge the PICSL imaging facility of the  
681 CIML (ImagImm), member of the national infrastructure France-BioImaging supported by the  
682 French National Research Agency (ANR-10-INBS-04). This project has also received funding  
683 from the European Union Horizon 2020 Research and Innovation Programme under the Marie

684 Skłodowska-Curie grant agreement No 765426 (TeraApps). This project has received fund-  
685 ing from the European Union's Horizon 2020 research and innovation programme under grant  
686 agreement No 964203 (FET-Open LINKS project).

## 687 **Authors Contributions**

688 M.L., Y.M., M.G. have been crucial for the success of the project. M.L. designed and per-  
689 formed all the experiments in Marseille regarding diffusion, he fixed the problem of operating  
690 the FCCS at high concentrations, and made the successful choice of the proteins to be studied.  
691 M.G. performed all the theoretical modelling and the related Molecular Dynamics and Monte  
692 Carlo numerical computations. Y.M. and S.R. carried out the experiments in Montpellier con-  
693 cerning THz-spectroscopy using the rectenna sensor and the micro-wire probe, both used for  
694 intramolecular collective vibration and frequency shift measurements. I.N. participated in the  
695 project from its very beginning many years ago paving the way to the present findings and  
696 suggested that ED forces could be detected through the frequency shift reported here. E.F. par-  
697 ticipated in the project from its very beginning and contributed the theoretical part of the paper.  
698 S.M. and D.M. gave fundamental support to perform the FCS and FCCS experiments. P.F., F.T.  
699 and L.V. participated in the project supporting it since its very beginning many years ago. J.S.  
700 contributed on the biophysical and biochemical aspects of the work. J.T., with the support of  
701 D.C. and S.R., conceived, designed and built the experimental setup in Montpellier and super-  
702 vised the experiments. M.P., in quality of project leader, initiated this research many years ago  
703 and designed, supervised and intervened in all the theoretical and experimental aspects of the  
704 project. All the authors contributed to the discussion and to the analysis of the results. M.P.  
705 wrote the paper with the help of J.T., D.M., J.S., M.G., M.L., S.R., E.F., L.V..

706 **Data Availability**

707 The data that support the findings of this study are available from the corresponding authors  
708 upon request. Theoretical models to interpret the experimental outcomes, as well as videos  
709 showing the formation of clusters, are available in the online version of the paper.

710 **Code Availability**

711 The codes that are used in this study are available from the corresponding authors upon request.

712 **Corresponding author**

713 Correspondence and requests for materials should be addressed to M.P. and J.T.

714 **Competing interests**

715 The authors declare no competing financial interests.

716 **Supplementary Materials**

717 Additional Experimental Data

718 Theoretical interpretation of the experimental results

719 Fig S1 - S22

720 **Online also:**

721 Movies S1 - S4